Probing Excited Electronic States Using Vibrationally Mediated Photolysis: Application to Hydrogen Iodide†

Jon P. Camden, Hans A. Bechtel, Davida J. Ankeny Brown, Andrew E. Pomerantz, and Richard N. Zare*

Department of Chemistry, Stanford University, Stanford, California 94305-5080

Robert J. Le Roy

Guelph-Waterloo Centre for Graduate Work in Chemistry and Biochemistry, University of Waterloo, Waterloo, Ontario N2L 3G1, Canada

Received: March 2, 2004; In Final Form: April 22, 2004

We measure branching ratios and anisotropy parameters for the photolysis of HI(v=2,J=0) → H + I($^2P^\circ_{1/2}$)/I($^2P^\circ_{3/2}$) over the wavelength range 297−350 nm. HI is prepared in the $v = 2$, $J = 0$ rovibrational level using direct IR absorption, and the H-atom photofragments are probed with resonance enhanced multiphoton ionization coupled with core-extraction time-of-flight mass spectrometry. The new branching ratio measurements disagree with predictions obtained from ab initio calculations and from the results of an empirical analysis based on experimental values of the HI/DI(v=0) absorption cross sections and branching ratios. Thus, we combine our new data with all existing absorption coefficient and branching fraction data for HI/DI in a global analysis that provides a new empirical determination of the final-state potential curves and transition moment functions for the four excited electronic states contributing to the A-band UV absorption continuum of HI. This analysis yields two models for the radial dependence of the excited state potential energy curves and transition dipole moment functions. The existing data cannot differentiate these models, but this work identifies a range of experiments that would do so. More generally, we demonstrate that photodissociation of vibrationally excited molecules is a sensitive probe of the repulsive excited electronic states encountered in bound-free transitions.

I. Introduction

Consider the unimolecular dissociation of a molecule when it absorbs a photon with sufficient energy to cleave a bond: the mechanism of this process and the resulting products are subtle probes of the forces at work in the excited electronic state or states prepared by the radiation field. Determining the mechanism and the photodissociation products, however, is not a trivial task, because several dissociation channels are often available. Questions that often arise include: what photofragments are formed? In what quantum states are they formed? What are the product vector correlations of these states; e.g., how does the velocity of the recoiling fragment point with respect to the direction of linear polarization of the light beam? In 1971 Jonah, Chandra, and Bersohn[1] used a method of "photolysis mapping" to begin addressing these very questions in the photolysis of $Cd(CH_3)_2$. The anisotropy of the Cd atoms with respect to the electric vector of the photolysis light was measured by allowing Cd to deposit on a glass hemispherical cell. From these measurements Bersohn and co-workers succeeded in making the first determination of the photoproduct angular distribution. They were able to conclude that the transition moment must be perpendicular to the C−Cd−C molecular axis of $Cd(CH_3)_2$.

This experiment and others confirmed that the photofragment angular distribution from a one-photon photodissociation event using linearly polarized light is given by[2,3]

$$I(\theta) = \frac{\sigma}{4\pi}[1 + \beta P_2(\cos\theta)] \qquad (1)$$

where θ is the angle between the electric vector of the light and the velocity vector of the product, σ is the partial cross section for the dissociation product, $P_2(x)$ is the second-order Legendre polynomial, and β is the anisotropy parameter. Within the axial recoil approximation, $\beta = -1$ corresponds to a perpendicular transition whereas $\beta = +2$ corresponds to a parallel transition. Since these early investigations, the union of detailed, high-quality experimental data with the most recent theoretical calculations has deepened our understanding of the immense complexities associated with the seemingly simple processes involved in molecular photodissociation.

In recent reviews, Crim[4,5] describes the power of vibrationally mediated photodissociation[6] to influence the outcome of a photodissocation event and unravel the complex interactions in the excited electronic states. Furthermore, as Figure 1 illustrates for the specific case of HI, vibrational excitation of molecules in the ground electronic state is a simple way to explore regions of the potential energy surface that are normally inaccessible. Although the information provided by such experiments should be a stringent test of available theories and enhance our understanding of excited electronic states, only a few studies[7−9] have considered the effect of vibrational excitation on the photodissociation dynamics of HX molecules. Such investigations are important to provide a testing ground for concepts that

† Part of the special issue "Richard Bersohn Memorial Issue".

* Corresponding author. E-mail: zare@stanford.edu.

10.1021/jp049051z CCC: $27.50
Published on Web 06/08/2004

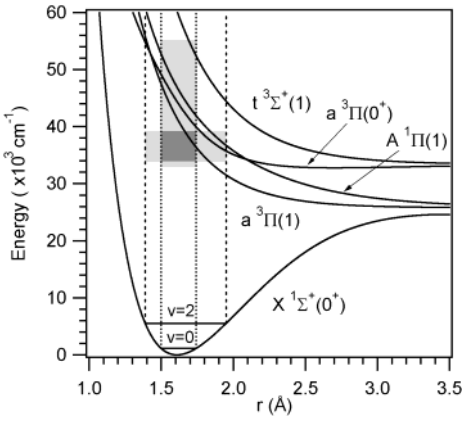

Figure 1. Empirical potential energy curves[43] for the lowest electronic states of HI labeled according to the historic Hund's case (a) notation. The dotted and dashed lines demarcate the $v = 0$ and $v = 2$ Franck−Condon regions, respectively. The vertical shaded box illustrates the region probed by previous $v = 0$ measurements and the horizontal shaded box illustrates the region of the current vibrationally mediated experiments.

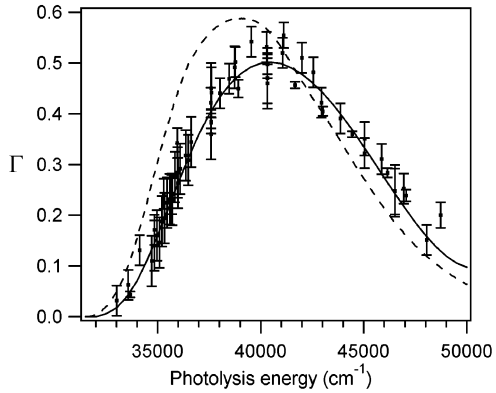

Figure 2. Experimental measurements and theoretical calculations of the branching ratio Γ for HI($v = 0$) photolysis. For clarity, no attempt is made to differentiate the experimental measurements (●) from refs 27−29, 31−33, 36−40, and 42. The dashed line represents ab initio calculations from ref 41, and the solid line is from the empirical analysis of ref 43.

might be applied to larger molecules. For example, what similarities can be drawn between photodissociation spectra of the HX series and the analogous CH_3X series? They also continue a long tradition of spectroscopic studies of the ground and excited electronic states of the hydrogen halides.

The hydrogen halides, HX (X = F, Cl, Br, I), are prototypical systems for investigating photodissociation dynamics because they provide an opportunity to explore nonadiabatic effects as well as the increasing spin−orbit coupling and decreasing bond strength from HF to HI. Excitation of HX molecules in the A-band continuum yields two different dissociation channels:

$$HX \rightarrow H\,(^2S) + X\,(^2P^\circ_{3/2}) \qquad (2)$$

$$HX \rightarrow H\,(^2S) + X^*\,(^2P^\circ_{1/2}) \qquad (3)$$

Here, we follow the standard convention of labeling the ground state ($^2P^\circ_{3/2}$) halogen atoms by X, and the spin−orbit-excited atoms ($^2P^\circ_{1/2}$) by X*. The branching ratio between these channels has been the subject of numerous experimental and theoretical investigations for HF,[8] HCl,[9−18] HBr,[19−22] and HI.[23−44] This ratio is often expressed in terms of Γ, which is defined as

$$\Gamma = \frac{\Phi_{X^*}}{\Phi_X + \Phi_{X^*}} \qquad (4)$$

where Φ_{X^*} and Φ_X are the quantum yields of X* and X, respectively. Experimentally, the photolysis of HI has received the most attention of the halogen halides, in part because the A-band absorption spectrum is red-shifted to more accessible wavelengths.

A. HI(v=0) Photodissocation. The UV absorption spectrum of HI is broad and featureless,[23,45−47] with the A-band beginning around 300 nm, peaking at ∼220 nm, and decreasing before the beginning of the B-band around 200 nm. In 1937 Mulliken[24] predicted that the observed A-band absorption was the result of Q ← N transitions, where N represents the $^1\Sigma^+(0^+)$ ground state and Q represents the group of states: $^3\Pi(1)$, $^1\Pi(1)$, and $^3\Pi(0^+)$. Although he also considered transitions to the T $^3\Sigma^+$-(1) and V $^1\Sigma^+(0^+)$ states, he predicted that the V state would show discrete band structure and that both the T and V states would be important only at higher energies. The empirically derived potential energy surfaces[43] of the N, Q, and T levels are shown in Figure 1. Here, we retain the historical Hund's case (a) notation but give Ω in parentheses because the presence of the heavy I atom results in a large spin−orbit splitting, which suggests that a Hund's case (c) description is likely better. In addition, we follow the convention of labeling triplet states with lower case letters, which was not used by Mulliken. The a $^3\Pi$-(0^+) ← X $^1\Sigma^+(0^+)$ transition is a parallel transition ($\Delta\Omega = 0$) and correlates to the H + I* channel, whereas the other two Q ← N transitions, a $^3\Pi(1)$ ← X $^1\Sigma^+(0^+)$ and A $^1\Pi(1)$ ← X $^1\Sigma^+$-(0^+), are both perpendicular transitions ($\Delta\Omega = \pm 1$) and correlate to the H + I channel. Finally, the t $^3\Sigma^+(1)$ ← X $^1\Sigma^+(0^+)$ continuum at the blue end of the A-band is a perpendicular transition and correlates to the H + I* channel.

Although early attempts to measure the branching ratio Γ were made using photochemical methods,[25,26] the uncertainties in such indirect techniques were rather large. After these initial measurements, numerous other groups[27−33,36,37,44] made measurements of Γ and the spatial anisotropy parameter for the I and I* channels, i.e., β and β*, at a variety of wavelengths in the A-band. These measurements were generally consistent with Mulliken's prediction that I atoms arise from a perpendicular transition whereas I* atoms are formed only via a parallel transition, except at the blue end of the A-band where a perpendicular transition into the t $^3\Sigma^+(1)$ state grows in. Figure 2 summarizes the extensive experimental measurements and displays the most recent ab initio calculations[41] along with the results of a comprehensive empirical analysis by Le Roy et al.[43] The ab initio calculations of the branching ratios agree qualitatively with the experimental values, whereas the empirical analysis agrees quantitatively. We note that unlike the previous theoretical work of Levy and Shapiro[34] the studies mentioned here did not include nonadiabatic couplings, a point that will be addressed in more detail later.

B. Vibrationally Mediated Photolysis of HX. Theoretical calculations on vibrationally excited HCl,[9,10] HBr,[21] and HI[35,41,48,49] have shown that the variation of Γ reflects the nodes in the ground electronic state vibrational wave functions. In the case of HI, calculations[35,41,48,49] predict that competition between the different Q ← N transitions could be exploited to control the spin−orbit branching ratio by preparing an initial vibrational state and tuning the photolysis wavelength to favor production of either I or I*. The implementation of these methods to influence the branching ratio rely on accurate knowledge of the

excited-state potentials and transition dipole moment functions that are probed in this work.

Experimentally, the photodissociation dynamics of vibrationally excited HX molecules have been mostly neglected with a few exceptions: Zhang et al.[8] determined Γ for the 193.3 nm photolysis of HF(v=3); Regan et al.[9] measured Γ for the photodissociation of HCl(v=1,J=0,5), HCl(v=2,J=0,11), and HCl(v=3,J=0,7) at ~235 nm; and Zittel and Little[7] compared the relative absorption cross-sections of HBr(v=1) and HBr(v=0) at 258.9 nm. These studies, though pioneering, used only one photolysis wavelength, therefore limiting the range over which the excited-state potentials are probed. To our knowledge, no measurements exist of Γ or β and β* for vibrationally excited HX molecules over a range of photolysis wavelengths. Moreover, there have been no measurements of vibrationally excited HI molecules, despite the extensive effort that has been made to obtain accurate values for the excitation energy dependent ϵ (molar absorption coefficients), Γ, β, and β* for HI/DI(v=0).

In this article, we report values of Γ, β, and β* for the photolysis of a single rovibrational state of hydrogen iodide, HI(v=2,J=0), in the red region of the A-band (297−350 nm). These measurements indeed show that vibrational excitation can lead to channel control in the I*/I branching ratio. Because none of the recent theoretical calculations[41,43] agree quantitatively with the new HI(v=2, J=0) data, we develop improved potential energy curves and transition moment functions (TMFs) to describe the entire experimental data on HI and DI photolysis. In addition, we demonstrate that vibrationally mediated photolysis is a powerful and sensitive tool for probing the potential energy surfaces and transition dipole moment functions for continuum transitions.

II. Methods and Procedures

A. Experimental Details. Figure 3 shows a schematic of the experimental apparatus, which has been described in detail elsewhere.[50] Here we present only a brief summary of the instrument and details important to the current experiments. A 1:20 mixture of hydrogen iodide, obtained by standard synthetic procedures,[51] and helium (Liquid Carbonic, 99.995%) is expanded from a pulsed nozzle (General Valve, Series-9) into the extraction region of a linear Wiley−McLaren time-of-flight (TOF) spectrometer.[52] The state preparation, photolysis, and product detection are accomplished using three different laser beams that intersect the expansion approximately 1 cm below the nozzle orifice. HI is first prepared in the $v = 2$, $J = 0$ level by direct IR absorption near 2.3 μm. The IR light, focused by a $f = 65$ cm CaF_2 lens into the extraction region, is generated by difference frequency mixing the fundamental of an injection seeded Nd^{3+}:YAG laser (Continuum, PL9020) with the ~725 nm output of a dye laser (Continuum, ND6000, Exciton: LDS 750) to make light around 2.3 μm. This light is amplified in an optical parametric amplification (OPA) stage to produce ~20 mJ of linearly polarized tunable radiation with a bandwidth of ~0.15 cm^{-1}. The line positions of the P and R branches of the HI(v=2) vibrational level are found using standard photoacoustic spectroscopy techniques. Because the current measurements rely on a randomly oriented sample in the lab frame, we pump the P(1) transition to avoid any bond axis or rotational alignment of the vibrationally excited HI molecules.[53] Furthermore, we verify that we are in the linear absorption regime, thereby avoiding any anomalous saturation effects, by ensuring the line width of the P(1) transition is laser bandwidth limited.

After a delay of 5−10 ns, the photolysis beam dissociates the vibrationally excited HI molecules. This light, tunable between 297 and 350 nm, is generated by frequency doubling the output of a Nd^{3+}:YAG (Continuum, PL8020) pumped dye laser (Spectra Physics, PDL-3, Exciton: LDS 698, DCM, Rhodamine 640, Rhodamine 610) in a BBO crystal to produce 2−4 mJ/pulse. The resulting H atoms are then probed after another 5−10 ns delay using 3+1 resonance enhanced multiphoton ionization (REMPI) on the 2p $^2P^\circ \leftarrow$ 1s ^2S transition around 365 nm. The probe light is generated by doubling the output of a Nd^{3+}:YAG (Spectra Physics, DCR-2A) pumped dye laser (Lambda Physik, FL2002, Exciton: LDS751) in BBO. The large photolysis and IR focal volume, small probe focal volume, and small time delay between the photolysis and probe lasers ensure that there is no bias arising from the faster moving products flying out of the detection region.

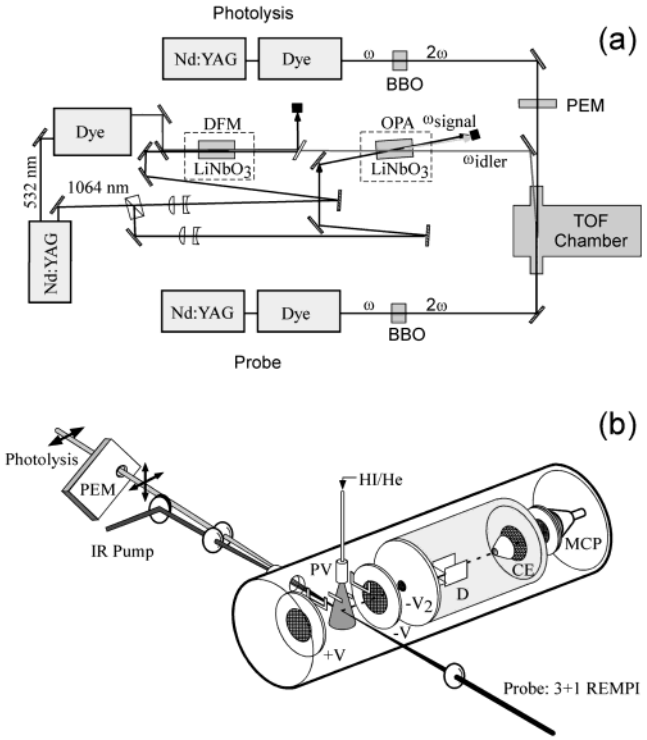

Figure 3. Experimental schematic. (a) Block diagram of the laser systems used to generate the IR, photolysis, and probe light. The IR is generated by difference frequency mixing, DFM, and optical parametric amplification, OPA. The photolysis and probe light is generated by frequency doubling in BBO the output of a dye laser. (b) Schematic of the Wiley−McLaren TOF used: D = deflection plates, CE = core extractor, MCP = multichannel plates, and PV = pulse valve.

The branching ratio and anisotropy parameters are obtained using the well-established core-extraction technique[50] coupled with space-focused TOF mass spectrometry. In this technique the ions are allowed to spread in time according to their initial velocities. Ions with velocity components perpendicular to the flight axis are rejected by the core extractor to simplify the data analysis. The mass spectrometer extraction voltages are set at 40 V/cm to give a resolution of ~1300 m/s for the H atom, which is sufficient to resolve the different dissociation channels. The direction of the linearly polarized photolysis beam is rotated between parallel and perpendicular to the TOF axis on an every-other-shot basis using a photoelastic modulator (PEM-80, Hinds International Inc). The resultant signals are combined to give the isotropic, $I_{iso} = 2I_\perp + I_{||}$, and anisotropic, $I_{aniso} = 2(I_{||} - I_\perp)$, TOF profiles, which are related to the speed-dependent population and speed-dependent lab-frame spatial anisotropy, $\beta(v)$, of the ions, respectively.[50] The purity of the photolysis polarization is confirmed by placing a polarizer after the PEM

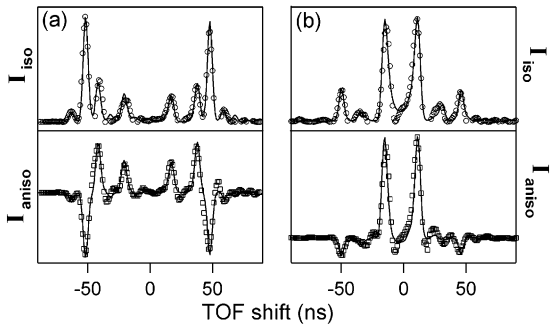

Figure 4. Experimental isotropic I_{iso} (○) and anisotropic I_{aniso} (□) core-extracted TOF profiles obtained from the photolysis of HI(v=0,$J\leq$3) and HI(v=2,J=0) at (a) 297 nm and (b) 350 nm. The solid black line is the fit as described in the text. The isotropic and anisotropic TOF profiles are not presented on the same scale for clarity.

and ensuring that signal is not observed when the photolysis polarization is crossed. The PEM is adjusted for each photolysis wavelength.

The spin−orbit splitting of the iodine atom is quite large (7605 cm^{-1}), and the vibrational energy of HI(v=2), 4380 cm^{-1} above the zero point energy, is about half of this value. Thus, there are four distinct channels listed in order of increasing translational energy of the H atom.

$$HI(v=0,J) \rightarrow H + I^* \quad (a)$$

$$HI(v=2,J=0) \rightarrow H + I^* \quad (b)$$

$$HI(v=0,J) \rightarrow H + I \quad (c)$$

$$HI(v=2,J=0) \rightarrow H + I \quad (d)$$

We fit the isotropic and anisotropic TOF profiles using three or four basis functions generated by a Monte Carlo simulation[50] to obtain the lab-frame speed distribution and β(v). Figure 4 displays the isotropic and anisotropic core-extracted TOF profiles for the 297 and 350 nm TOFs and the corresponding simulated fits. Peaks with the largest positive and negative TOF shifts correspond to the fastest products, in this case channel (d), moving initially toward and away from the detector, respectively. Similar data are obtained for the other wavelengths studied.

As a check on our fitting program, we also calculate the relative peak areas of the isotropic and anisotropic profiles because under perfect core-extraction conditions, β is determined by

$$\beta(v) = I_{aniso}/I_{iso} \quad (5)$$

where I_{aniso} and I_{iso} are the integrated values of the signal for each lab speed, v. Both methods give identical values within their uncertainties. We also confirm that the H atom spatial anisotropy $\beta = -1$ for our measurements of HI(v=0) photolysis at 324 nm, where there are only two accessible states, a $^3\Pi(1)$ and A $^1\Pi(1)$, and both correlate to I atoms via a perpendicular transition. Last, we note that the H atoms coincident with both I and I* are detected simultaneously, thus avoiding any bias introduced by separate measurements. The branching ratio of HI(v=0) photolysis at 297 nm is found to be in good agreement with the corrected values of Regan et al.[40]

B. Empirical Analysis. The empirical analysis reported here is performed using the same quantum simulation/fitting program[54] and the comprehensive data set of ref 43 supplemented by the new $v = 2$, $J = 0$ branching ratio measurements of Table 1. Thus, only a brief description of the theoretical methods is provided. The analysis is based on a quantum mechanical simulation of the total absorption coefficient and branching ratio data. A least-squares fitting procedure optimizes the parameters characterizing the analytic models for the various final-state potential energy functions.

TABLE 1: Experimental Values for the Branching Ratio Γ and Anisotropy Parameters β and β^* for HI(v=2,J=0) Photolysis[a]

wavelength (nm)	Γ	β	β^*
297	0.64 ± 0.05	−0.93 ± 0.12	2.08 ± 0.12
306	0.76 ± 0.04	−0.99 ± 0.12	1.96 ± 0.22
313.88	0.80 ± 0.04	−0.96 ± 0.12	2.03 ± 0.26
320	0.79 ± 0.06	−0.93 ± 0.15	1.97 ± 0.12
330	0.81 ± 0.05	−1.09 ± 0.26	1.80 ± 0.23
340	0.61 ± 0.05	−1.10 ± 0.17	1.84 ± 0.20
350	0.26 ± 0.04	−1.05 ± 0.11	1.95 ± 0.12

[a] The stated uncertainty is the statistical 95% confidence interval calculated from replicate measurements.

Following the approach of ref 43, the potential energy functions for the A $^1\Pi(1)$, a $^3\Pi(1)$, and t $^3\Sigma^+(1)$ states are represented by the simple exponential function

$$V_{exp}(r) = \mathscr{D}_s + A_s e^{-\beta(y_p)(r-r_x)} \quad (6)$$

and the a $^3\Pi(0^+)$ state is represented by the "extended Morse oscillator" (EMO) function[55]

$$V_{EMO} = [\mathscr{D}_s - \mathscr{D}_e] + \mathscr{D}_e[e^{-\beta(y_p)(r-r_x)} - 1]^2 \quad (7)$$

Here, $\mathscr{D}_s$ is the energy at the asymptote of electronic state s, r_x is a reference distance chosen to lie near the ground-state equilibrium distance in the middle of the Franck−Condon overlap region, r_x = 1.609 Å, and the exponent coefficient

$$\beta(y_p) = \beta_0 + \beta_1 y_p + \beta_2 y_p^2 + ... \quad (8)$$

is defined as an expansion in the dimensionless radial variable $y_p = [r^p - r_x^p]/[r^p + r_x^p]$. In the EMO function, eq 7, $\mathscr{D}_e$ is the well depth and r_e is the radial position of the shallow minimum. Because this predicted shallow potential minimum is outside the region probed by HI(v=0) photodissociation studies, $\mathscr{D}_e$ is fixed at the ab initio value $\mathscr{D}_e$ = 600 cm^{-1}. Similarly, without further experimentation we fix the power defining the radial distance variable as $y_p(r)$ with $p = 8$.[43]

In earlier work[43] the photodissociation spectra originating in a $v = 0$ vibrational level was found to be quite insensitive to the radial shape of a transition dipole moment function because of intimate correlation with the position and shape of the final-state potential curve. This restriction is lifted, however, if the data depend significantly on absorption from vibrationally excited levels.[56] As a result, we consider two types of models: (1) the transition moment functions are linearly scaled versions of the ab initio functions,[43] and (2) the transition moment functions are represented by empirical expansions in powers of the radial variable y_p

$$M(r) = \sum_{i=0} c_i y_p^i \quad (9)$$

We cannot expect that the current data, lying at the red end of the photolysis region, will give new insight regarding transitions to the t $^3\Sigma^+(1)$ state, which is only significant in the extreme blue region of the A-band absorption. Thus, we choose to retain

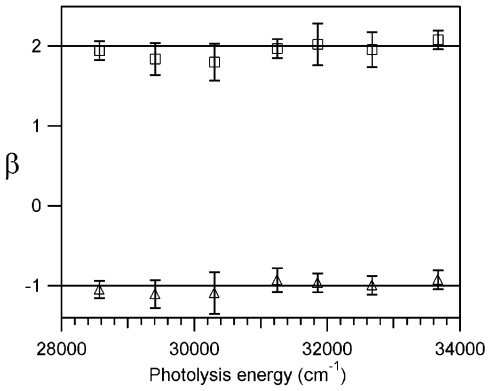

Figure 5. β^* parameter for the HI(v=2,J=0) → H + I* channel (□) and β parameter for the HI(v=2,J=0) → H + I channel (△). Solid lines represent limiting values (−1, +2) for the anisotropy parameter β.

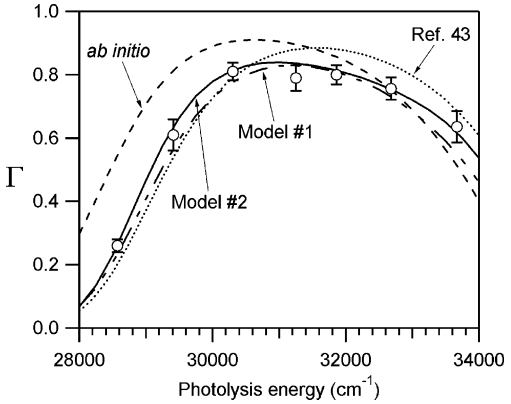

Figure 6. Branching ratio $\Gamma = \Phi_{I^*}/(\Phi_I + \Phi_{I^*})$ for HI(v=2,J=0) photolysis plotted as a function of excitation frequency (○). Error bars represent 95% confidence limits obtained from replicate measurements. The curves are the prediction of ref 43 (dotted line), ab initio calculations from ref 41 (dashed line), and the two new models presented in this work: model 1 (dash-dot-dot line) and model 2 (solid line).

the scaled ab initio TMF for the t $^3\Sigma^+(1)$ state with the scaling factor fixed at c_0(t $^3\Sigma^+(1)$) = 1 as in ref 43.

III. Results and Discussion

A. Spatial Anisotropy. Figure 5 displays the measured channel-specific anisotropy parameters, and Table 1 tabulates these values. Several features are immediately obvious. First, the β values obtained for the HI(v=2,J=0) → H + I channel indicate a pure perpendicular transition within experimental uncertainty over the entire excitation energy range studied here. This result is consistent with previous studies[28,30,32,33,36,38,39] of HI(v=0) photolysis and lends support to the picture that excitation to the a $^3\Pi(1)$ and A $^1\Pi(1)$ states via a perpendicular transition leads to a prompt dissociation and production of ground-state I. We note that the axial recoil approximation should be rigorous because the vibrationally excited photolysis signal results from HI(v=2) prepared in the J = 0 rotational level.

There has been some disagreement, however, among previous HI(v=0) experimental measurements[28,30,32,33,36,38,39] and theoretical predictions[34,41,43]concerning the value of β^* for the HI(v=0) → H + I* channel. These results have raised questions about the extent of nonadiabatic coupling present between the excited states. The recent studies of Gendron et al.[39] and Langford et al.,[38] however, show that I* production in the A-band arises primarily from the parallel (β^* = +2) transition [a $^3\Pi(0^+)$ ← X $^1\Sigma^+(0^+)$], as suggested by Mulliken. The possibility of a small contribution from another state of different symmetry, however, has not been ruled out experimentally because the value obtained for β^* at a variety of wavelengths is often less than 2 but still includes the limiting value (β^* = 2) within its uncertainty.

Several speculations consistent with the experimental data had been previously proposed. Langford et al.[38] hypothesized that the t $^3\Sigma^+(1)$ state, predicted by Mulliken to be of higher energy than the Q group, might in fact be low enough in energy to contribute to the A-band absorption. The t $^3\Sigma^+(1)$ ← X $^1\Sigma^+(0^+)$ transition is perpendicular and correlates to I* products that would lead to a nonlimiting β parameter. In 2000 Alekseyev et al.[41] performed an ab initio study of the excited-state potentials of HI and concluded that (1) the t $^3\Sigma^+(1)$ state would be accessible only at excitation energies greater than 50 000 cm^{-1}, confirming Mulliken's initial predictions, and (2) nonadiabatic couplings are unimportant. A later study by Balakrishnan et al.[57] explored the spin-rotational coupling of the A $^1\Pi(1)$ and a $^3\Pi(0^+)$ states and found it to be negligible. Our data are consistent with this picture and further support the notion that I* production in the A-band results from a pure parallel transition to the a $^3\Pi(0^+)$ state. Therefore, in our opinion the available theoretical and experimental data support the current view[41,43,57] that (1) nonadiabatic interactions, if present, are small in the red region of the A-band and (2) the t $^3\Sigma^+(1)$ state is not accessible at these energies, even upon excitation of HI to its first overtone, which extends the Franck−Condon region.

B. Branching Ratios. The experimentally determined value of Γ for HI(v=2,J=0) photolysis over the range of 28 000 to 34 000 cm^{-1}, shown in Figure 6, is very different than that observed for the HI(v=0) photolysis, shown in Figure 2. Indeed, the prediction first made by Kalyanaraman and Sathyamurthy[35] and later by other groups[41,48,49] that Γ could be controlled by vibrational excitation is confirmed. Over the wavelength range considered here, Γ can range from ∼0.3 to 0.8, indicating that mainly I or mainly I* can be produced from photolysis of HI(v=2), in contrast to the photolysis of HI(v=0) where the maximum value of Γ is ∼0.5 (Figure 2). To gain a deeper understanding of these differences, we now examine the relation of previous models to our HI(v=2,J=0) data and as a result propose several refinements.

Figure 6 shows the predicted Γ values derived (1) from the most recent ab initio calculations[41] and (2) from the empirical analysis of Le Roy et al.[43] based only on HI(v=0)/DI(v=0) data. Although both calculations agree qualitatively with the experimental measurements of HI(v=2), neither agree quantitatively. Clearly, the current potential energy curves and transition moment functions are not accurate enough to describe completely the photodissociation dynamics of HI. Consequently, we attempt to develop improved potential energy curves and transition moment functions using a comprehensive empirical analysis of all the available experimental data for HI and DI.

In the resulting weighted least-squares fits (see section II.B), the quality of the fit is represented by the dimensionless root-mean-square residual

$$\mathrm{RMSR} = \{(1/N_\mathrm{d})\sum_{i=1}^{N_\mathrm{d}}[(Y_\mathrm{calc}(i) - Y_\mathrm{obs}(i))/u(i)]^2\}^{1/2} \quad (10)$$

where N_d is the number of experimental data and $u(i)$ is the estimated uncertainty in datum i. Note that one can use this quantity to indicate the quality of fit to a subset of data (such as the v = 2, J = 0 branching ratios) as well as for the overall

TABLE 2: RMSR Values for Selected Models Considered in the Global Reanalysis of the HI/DI(v=0) Absorption Measurements and Branching Ratio Data from Ref 43 Including the New HI(v=2,J=0) Branching Ratio Data

	ref 43	model 1	model 2
RMSR, global	0.93	0.82	0.85
RMSR, ($\Gamma_{v=2}$)	1.52	0.96	0.53

fit. The first column of Table 2 gives the RMSR values for the entire data set, including 164 previous data points as well as the current HI(v=2,J=0) measurements, obtained with the potential energy and transition moment functions determined previously.[43] A refit of the full 14-free-parameter model used in ref 43 was performed by including the new data presented here; however, it suffered the same types of systematic discrepancies seen for the ref 43 curve in Figure 6. Thus, it is clear that obtaining good agreement with our new $v = 2$, $J = 0$ branching ratios requires significant extensions of the best existing empirical model[43] for this system. Therefore, fits to the full data set using a wide range of models for the final-state potentials were performed. In this phase all four transition moment functions were represented by spline functions through the ab initio points,[41] and each was multiplied by an empirical scaling factor. However, none of these models yielded a satisfactory representation of the new $v = 2$ branching ratios. This suggested that a more sophisticated treatment of the transition moment functions, rather than of the final state potentials, was needed to match the HI(v=2,J=0) measurements.

After considerable experimentation, we converged on two models defined by the parameter sets listed in Table 3, which we will refer to as models 1 and 2. The most important difference between them is that model 1 uses an empirical linear function for the transition moment function into the a $^3\Pi(0^+)$ state and scaled ab initio functions for the others, whereas model 2 uses empirical functions linear in the variable $y_8(r)$ for the transition moments into both the A $^1\Pi(1)$ and a $^3\Pi(0^+)$ states. Additionally, the value of r_e is allowed to vary in model 1, whereas it is fixed at the ab initio value[41] of 2.7 Å in model 2. Figure 7 illustrates the quality of agreement of these two models with the five types of experimental data used in the analysis. Both models 1 and 2 give a significantly better overall quality of fit than the best of the previous models, as indicated by the RMSR values in Table 2 and the agreement seen in Figure 6.

Figure 8 compares the potential energy and transition moment functions of the two new models and deserves some comment. The main difference between these models is the use of an empirical linear function rather than a scaled ab initio transition moment function for the A $^1\Pi(1)$ state. In view of the rather different shapes of the A $^1\Pi(1)$ transition moment functions across the FC region for models 1 and 2, it is no surprise that

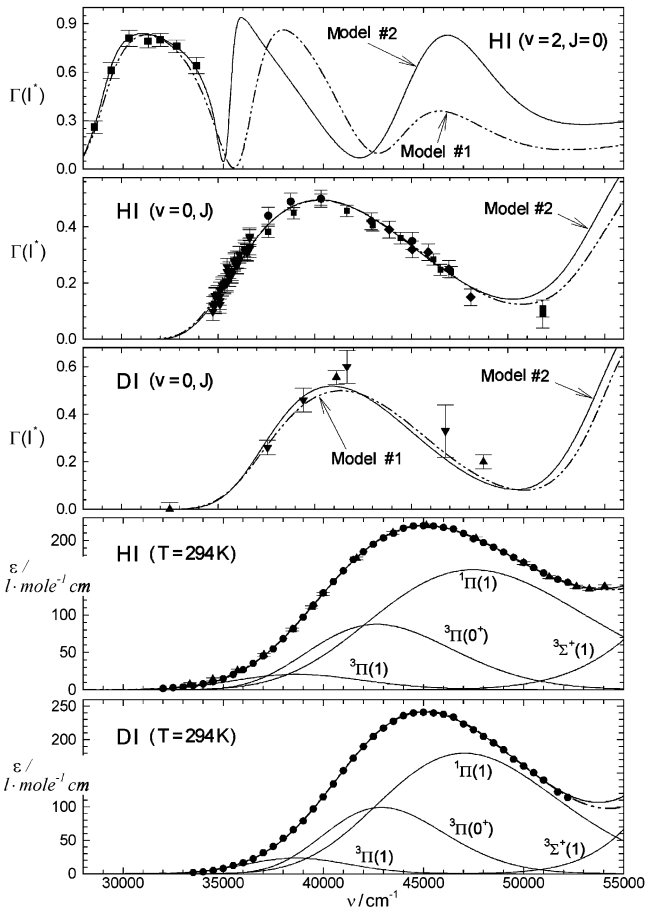

Figure 7. Comparison between experiment (points) and the fits obtained using model 1 (dash-dot-dot lines) and model 2 (solid lines), which are defined by the parameters in Table 3. From top to bottom, the data include HI(v=2,J=0) branching ratios, HI(v=0,J) branching ratios, DI(v=0,J) branching ratios, HI(T=294K) absorption cross sections, and DI(T=294K) absorption cross sections.

the associated A $^1\Pi(1)$ state potentials differ significantly. It is surprising, however, that the potential energy and transition moment functions for the a $^3\Pi(1)$ state also change considerably. This result illustrates the high degree of correlation among the parameters defining the models and accounts for our inability to recommend one model over the other. We note that, except for the transition moment function for a $^3\Pi(0^+)$, the transition moment functions and potentials from model 1 closely resemble those from ref 43.

Prior to the present work, all experimental efforts have been directed at obtaining accurate values of Γ and ϵ for the HI/DI(v=0) photodissociation spectra. Both models 1 and 2 give

TABLE 3: Parameters Defining the Potential Energy and Transition Moment Functions for HI and DI[a]

	A $^1\Pi(1)$		a $^3\Pi(0^+)$		a $^3\Pi(1)$		t $^3\Sigma^+(1)$	
model	1	2	1	2	1	2	1	2
D_s/cm^{-1}	25778	25778	33381	33381	25778	25778	33381	33381
g_u	2	2	1	1	2	2	2	2
form	expt	expt	EMO	EMO	expt	expt	expt	expt
A_s/cm^{-1}	20873 (±110)	20384 (±68)	*b*	*b*	15188 (±290)	12823 (±220)	27690 (±200)	26830 (±190)
β_0/Å^{-1}	2.304 (±0.044)	2.945 (±0.042)	1.6323 (±0.051)	1.51592 (±0.0036)	2.965 (±0.79)	2.495 (±0.11)	2.6	2.6
β_1/Å^{-1}	−0.437 (±0.093)	−0.260 (±0.11)	0.056 (±0.035)					
c_0	0.978[c] (±0.021)	0.4623 (±0.0064)	0.4072 (±0.0068)	0.4131 (±0.0058)	1.329[c] (±0.091)	0.823[c] (±0.062)	1.0[c]	1.0[c]
c_1		−0.613 (±0.027)	0.069 (±0.043)	−0.130 (+0.033)				

[a] 95% confidence limit uncertainties are given in parentheses. The potential function exponent coefficients expansion variable is $y_8(r)$, and the fit yields f_e(DI) = 1/0.9632 (±0.0039) for model 1 and 1/0.9365 (±0.0033) for model 2. See text or ref 43 for details. [b] EMO potential form with fixed well depth $\mathscr{D}_e$ = 600 cm^{-1}, and with r_e = 2.63892(±0.032) Å for model 1 and r_e fixed at 2.7 Å for model 2. [c] Transition moment defined as cubic spline through ab initio values from ref 41, multiplied by this scaling factor c_0.

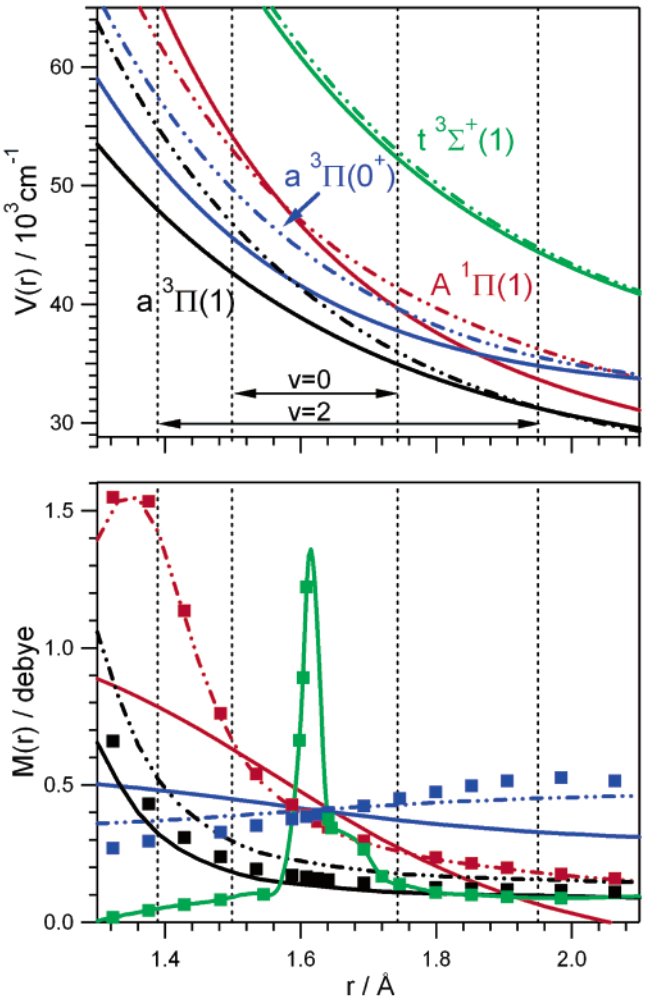

Figure 8. Comparison of the excited-state potential energy curves (upper panel) and transition dipole moment functions (lower panel) for model 1 (dash-dot-dot line), model 2 (solid line), and the ab initio points calculated in ref 41 (solid squares). The different states are grouped according to color: black, a $^3\Pi(1)$; blue, a $^3\Pi(0^+)$; red, A $^1\Pi(1)$; green, t $^3\Sigma^+(1)$. The transition moment functions are given in units of Debye, where 1 D = 3.33564 × 10^{-30} C·m. The parameters defining the potential energy functions and transition moment functions are listed in Table 3 and described in the text.

predictions that quantitatively agree with all previous experiments (Figure 7), but they yield significantly different potential energy curves and TMFs, even in the $v = 0$ FC region (Figure 8). Although the distinctly smaller value of RMSR($\Gamma_{v=2}$) given in Table 2 suggests that model 2 is preferred, relative to the uncertainties in our data, we cannot unequivocally recommend one model over the other. However, the total absorption cross sections and branching ratio predictions for models 1 and 2 for HI (v=0−4,J=0) shown in Figure 9 reveal that photodissociation studies of vibrationally excited HI would differentiate them. In particular, measurement of the state selected absorption cross section for the same vibrational state and excitation energies probed in this work would distinguish the two models.

Figure 9 demonstrates that accurate knowledge of the excited-state potentials and TMFs is critical to designing experiments that control the I/I* branching ratio. The mechanism of this control can be understood from the empirical analysis and experimental anisotropy parameter measurements presented above. Because this investigation supports the existing idea that nonadiabatic couplings between the excited states are small or nonexistent, the value of Γ is determined only by the partial absorption cross sections into the different electronic states

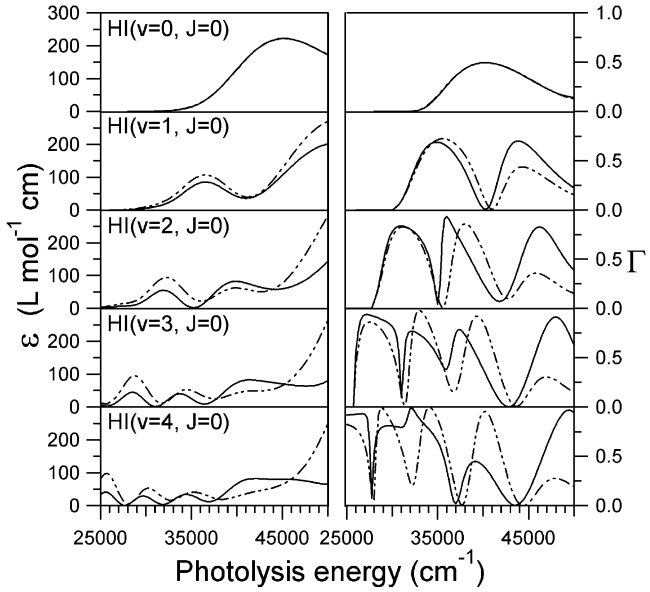

Figure 9. Predicted total absorption cross sections and branching ratios, Γ, for HI(v=0−4,J=0) photolysis obtained using model 1 (dash-dot-dot lines) and model 2 (solid lines). The models are indistinguishable in the regions where experimental measurements are available; however, significant differences between the models are observed in the absorption cross sections and branching ratios of higher vibrational states.

correlating to I and I*, respectively. In the current work, this competition is specifically between absorption to the a $^3\Pi(1)$, A $^1\Pi(1)$, and a $^3\Pi(0^+)$ states. Thus, although we demonstrate that excitation to $v = 2$ followed by dissociation around 310 nm leads to an inversion of the iodine spin−orbit states, we also demonstrate that the current description of the excited states is insufficient to make quantitative predictions about the photolysis from vibrational levels other than the ground state and other excitation energies. Additional experimental work is clearly needed to refine our knowledge of the HI A-band continuum.

IV. Synthesis

Conventional spectroscopic methods are capable of probing the shape and nature of bound molecular electronic states in extraordinary detail. To take an example relevant to this work, consider the accuracy and precision to which the parameters defining the HI X $^1\Sigma^+(0^+)$ state are known. A recent spectroscopic study[58] of HI aimed at determining the Born−Oppenheimer correction to the molecular Hamiltonian used 13 fitted parameters, which contain 4−10 significant figures, to characterize the X state. In contrast, repulsive states have received much less attention because they are more difficult to study owing to experimental difficulties and their lack of sharp spectral features. The problem seems to be intractable when there are many excited states and the possibility of nonadiabatic effects. Here we have proposed another method—vibrationally mediated photolysis—to aid in untangling such states and their couplings. Measurements of the state-selected absorption cross-sections as well as branching ratios should yield information capable of placing ever stricter constraints on the potential energy curves and transition dipole moment functions of the excited states. This information also allows detailed comparison with improved ab initio calculations.

In the specific case of HI, we have demonstrated channel control over the resulting photofragments. We note that this method of passive control, where a specific vibrational eigenstate

is prepared, is very different from that of coherent control.[59,60] This work demonstrates that a proper choice of photolysis wavelength and initial HI rovibrational state allows over 80% of the photolytic iodine atoms to be prepared in the spin−orbit-excited level, whereas if HI is photolyzed from its ground vibrational level only about 50% of the iodine atoms can be prepared in the spin−orbit-excited level. The mechanism of this control is elucidated, and Figure 9 illustrates the importance of having a detailed understanding of the excited states, to predict how one can obtain this control.

The qualitative agreement of previous ab initio[41] branching ratios and anisotropy parameters for HI(v=2) with the present results attests to the quality of those calculations. This level of agreement is rather remarkable because relativistic corrections had to be introduced in obtaining the potential energy curves and transition moment functions. However, the present HI(v=2,J=0) photolysis data do differ systematically from those predictions, which suggests that further improvements in the ab initio calculations are needed.

The experimentally determined photofragment angular distributions strongly support the picture that HI photolysis proceeds without significant coupling between the different excited electronic states. Thus, we were encouraged to make a global reanalysis in the same spirit as Le Roy et al.[43] using data for the photolysis of the HI vibrational ground state. We find from the global reanalysis that two empirical models are successfully able to reproduce all experimental data. Further experiments should be able to distinguish between these models and likely will lead to further improvements in the empirical fits. Indeed, Figure 9 illustrates many experiments that would be capable of differentiating between these models and elucidates the power of vibrationally mediated photolysis in providing more information about repulsive electronic states. Thus, for HI photolysis, despite so many years of study, the beat goes on.

Acknowledgment. J.P.C, H.A.B., and A.E.P. thank the National Science Foundation for graduate fellowships. H.A.B. also acknowledges Stanford University for the award of a Stanford Graduate Fellowship. Work at Stanford University is supported by the National Science Foundation under Grant No. 0242103 and at the University of Waterloo by the Natural Sciences and Engineering Research Council of Canada.

References and Notes

(1) Jonah, C.; Chandra, P.; Bersohn, R. *J. Chem. Phys.* **1971**, *55* (4), 1903.
(2) Zare, R. N.; Herschbach, D. R. *Proc. IEEE* **1963**, *51*, 173.
(3) Zare, R. N. *Mol. Photochem.* **1972**, *4*, 1.
(4) Crim, F. F. *Annu. Rev. Phys. Chem.* **1993**, *44*, 397.
(5) Crim, F. F. *J. Phys. Chem* **1996**, *100* (31), 12725.
(6) Schinke, R.; Engel, V.; Andersen, P.; Hausler, D.; Balint-Kurti, G. G. *Phys. Rev. Lett.* **1985**, *55*, 1180.
(7) Zittel, P. F.; Little, D. D. *J. Chem. Phys.* **1979**, *71* (2), 713.
(8) Zhang, J.; Riehn, C. W.; Dulligan, M.; Wittig, C. *J. Chem. Phys.* **1996**, *104* (18), 7027.
(9) Regan, P. M.; Ascenzi, D.; Brown, A.; Balint-Kurti, G. G.; Orr-Ewing, A. J. *J. Chem. Phys.* **2000**, *112* (23), 10259.
(10) Givertz, S. C.; Balint-Kurti, G. G. *J. Chem. Soc., Faraday Trans. 2* **1986**, *82*, 1231.
(11) Tonokura, K.; Matsumi, Y.; Kawasaki, M.; Tasaki, S.; Bersohn, R. *J. Chem. Phys.* **1992**, *97* (11), 8210.
(12) Alexander, M. H.; Pouilly, B.; Duhoo, T. *J. Chem. Phys.* **1993**, *99* (3), 1752.
(13) Gersonde, I. H.; Hennig, S.; Gabriel, H. *J. Chem. Phys.* **1994**, *101* (11), 9558.
(14) Adams, G. F.; Chabalowski, C. F. *J. Phys. Chem*. **1994**, *98* (23), 5878.
(15) Duhoo, T.; Pouilly, B. *J. Chem. Phys.* **1995**, *103* (1), 182.
(16) Zhang, D. H.; Dulligan, M.; Wittig, C. *J. Chem. Phys.* **1997**, *107* (5), 1403.
(17) Lambert, H. M.; Dagdigian, P. J.; Alexander, M. H. *J. Chem. Phys.* **1998**, *108* (11), 4460.
(18) Alexander, M. H.; Li, X.; Liyanage, R.; Gordon, R. *J. Chem. Phys.* **1998**, *231*, 331.
(19) Peoux, G.; Monnerville, M.; Duhoo, T.; Pouilly, B. *J. Chem. Phys.* **1997**, *107* (1), 70.
(20) Regan, P. M.; Langford, S. R.; Orr-Ewing, A. J.; Ashfold, M. N. R. *J. Chem. Phys.* **1999**, *110* (1), 281.
(21) Pouilly, B.; Monnerville, M. *Chem. Phys.* **1998**, *238*, 437.
(22) Baumfalk, R.; Buck, U.; Frischkorn, C.; Nahler, N. H.; Huewel, L. *J. Chem. Phys.* **1999**, *111* (6), 2595.
(23) Tingey, H. C.; Gerke, R. H. *J. Am. Chem. Soc.* **1926**, *48*, 1838.
(24) Mulliken, R. S. *Phys. Rev.* **1937**, *51*, 310.
(25) Cadman, P.; Polanyi, J. C. *J. Phys. Chem.* **1968**, *72* (11), 3715.
(26) Compton, L. E.; Martin, R. M. *J. Phys. Chem*. **1969**, *73* (10), 3474.
(27) Clear, R. D.; Riley, S. J.; Wilson, K. R. *J. Chem. Phys.* **1975**, *63* (4), 1340.
(28) Schmiedl, R.; Dugan, H.; Meier, W.; Welge, K. H. *Z. Phys. A* **1982**, *304*, 137.
(29) Brewer, P.; Das, P.; Ondrey, G.; Bersohn, R. *J. Chem. Phys*. **1983**, *79* (2), 720.
(30) VanVeen, G. N. A.; Mohamed, K. A.; Baller, T.; DeVries, A. E. *Chem. Phys.* **1983**, *80*, 113.
(31) Wight, C. A.; Leone, S. R. *J. Chem. Phys.* **1983**, *79* (10), 4823.
(32) Xu, Z.; Koplitz, B.; Wittig, C. *J. Phys. Chem* **1988**, *92*, 5518.
(33) Xu, Z.; Koplitz, B.; Wittig, C. *J. Chem. Phys.* **1989**, *90* (5), 2692.
(34) Levy, I.; Shapiro, M. J. Chem. Phys.**1988**, *89* (5), 2900.
(35) Kalyanaraman, C.; Sathyamurthy, N. *Chem. Phys. Lett.* **1993**, *209* (1, 2), 52.
(36) Kitsopoulos, T. N.; Buntine, M. A.; Baldwin, D. P.; Zare, R. N.; Chandler, D. W. *SPIE* **1993**, *1858*, 2.
(37) Heck, A. J. R.; Chandler, D. W. *Annu. Rev. Phys. Chem.* **1995**, *46*, 335.
(38) Langford, S. R.; Regan, P. M.; Orr-Ewing, A. J.; Ashfold, M. N. R. *Chem. Phys.* **1998**, *231*, 245.
(39) Gendron, D. J.; Hepburn, J. W. *J. Chem. Phys.* **1998**, *109* (17), 7205.
(40) Regan, P. M.; Ascenzi, D.; Clementi, C.; Ashfold, M. N. R.; Orr-Ewing, A. *J. Chem. Phys. Lett.* **1999**, *315*, 187.
(41) Alekseyev, A. B.; Liebermann, H. P.; Kokh, D. B.; Buenker, R. J. *J. Chem. Phys.* **2000**, *113* (15), 6174.
(42) Manzhos, S.; Loock, H.-P.; Bakker, B. L. G.; Parker, D. H. *J. Chem. Phys*. **2002**, *117* (20), 9347.
(43) Le Roy, R. J.; Kraemer, G. T.; Manzhos, S. *J. Chem. Phys.* **2002**, *117* (20), 9353.
(44) Betts, J. A. Ph.D. Thesis, California Institute of Technology, 1972.
(45) Huebert, B. J.; Martin, R. M. *J. Phys. Chem.* **1968**, *78* (8), 3046.
(46) Goodeve, C. F.; Taylor, A. W. C. *Proc. R. Soc. London, Ser. A* **1936**, *154* (881), 181.
(47) Ogilvie, J. F. *Trans. Faraday Soc.* **1971**, *67* (584), 2205.
(48) Gross, P.; Gupta, A. K.; Bairagi, D. B.; Mishra, M. K. *J. Chem. Phys.* **1996**, *104*, 7045.
(49) Fujisaki, H.; Teranishi, Y.; Nakamura, H. *J. Theor. Comput. Chem. 1* **2002**, (2), 245.
(50) Simpson, W. R.; Orr-Ewing, A. J.; Rakitzis, T. P.; Kandel, S. A.; Zare, R. N. *J. Chem. Phys.* **1995**, *103* (*17*), 7299.
(51) Schonbein, C. F. *Poggendofrs Ann.* **1849**, *78*, 516.
(52) Wiley, W. C.; McLaren, I. H. *Rev. Sci. Instrum*. **1955**, *26*, 1150.
(53) Zare, R. N. *Ber. Bunsen-Ges. Phys. Chem.* **1982**, *86*, 422.
(54) Le Roy, R. J.; Kraemer, G. T. A Computer Program for Calculating Bound→Continuum Transition Intensities for Diatomic Molecules. University of Waterloo Chemical Physics Research Report CP-650, 2002. The source code and manual for this program may be obtained from "Computer Programs" link on the www site http://leroy.uwaterloo.ca.
(55) Lee, E. G.; Seto, J. Y.; Hirao, T.; Bernath, P. F.; Le Roy, R. J. *J. Mol. Spectrosc.* **1999**, *194*, 197.
(56) Le Roy, R. J.; Macdonald, R. G.; Burns, G. *J. Chem. Phys*. **1976**, *65*, 1485.
(57) Balakrishnan, N.; Alekseyev, A. B.; Buenker, R. J. *Chem. Phys. Lett.* **2001**, *341*, 594.
(58) Coxon, J. A.; Hajigeorgiou, P. G. *J. Mol. Spectrosc.* **1991**, *150*, 1.
(59) Gordon, R. J.; Zhu, L.; Seideman, T. *Acc. Chem. Res.* **1999**, *32*, 1007.
(60) Zare, R. N. *Science* **1998**, *279* (5358), 1875.